Geochemistry Geophysics Geosystems G3
AN ELECTRONIC JOURNAL OF THE EARTH SCIENCES
Published by AGU and the Geochemical Society

Technical Brief
Volume 4, Number 4
22 April 2003
8302, doi:10.1029/2001GC000214
ISSN: 1525-2027

Testing the tracer ratio method for modeling active compositional fields in mantle convection simulations

Paul J. Tackley
Department of Earth and Space Sciences and Institute of Geophysics and Planetary Physics, University of California Los Angeles, 595 Charles Young Drive East, Los Angeles, California 90095, USA (ptackley@ucla.edu)

Scott D. King
Department of Earth and Atmospheric Sciences, Purdue University, 550 Stadium Mall Drive, West Lafayette, Indiana 47907, USA (sking@purdue.edu)

[1] Tracer methods are attractive for modeling compositional fields because they offer the potential of zero numerical diffusion. Composition is typically taken to be proportional to the absolute local concentration of tracers, but an increasingly popular method is to have "dense" and "regular" tracers with composition being equal to the local fraction of "dense" tracers. This paper tests this "ratio" method using established benchmarks and by comparing the performance of the two tracer methods and grid-based methods for simulating the long-term evolution of a convecting mantle with a thick, dense, stable layer. For this scenario the ratio method is found to have several advantages, giving sharp, stable long-term layering with no tracer settling, minimal statistical "noise" and low entrainment, even with only ~5 tracers per cell. The method is equally applicable to finite volume and finite element treatments of the underlying flow. Entrainment in grid-based advection methods is heavily dependent on resolution and numerical details, and is reduced ~1 order of magnitude by the filter proposed by A. Lenardic. Numerical determination of physically correct entrainment rates remains a challenging problem. Comparing tracer and grid based methods, the spatial pattern of the thermal and chemical fields appear to be converging on the finest grids; however the estimated entrainment differs significantly.

Components: 6488 words, 11 figures, 1 table.

Keywords: Mantle convection; chemical layering; tracer methods.

Index Terms: 8121 Tectonophysics: Dynamics, convection currents and mantle plumes; 1025 Geochemistry: Composition of the mantle; 8194 Tectonophysics: Evolution of the Earth: Instruments and techniques.

Received 21 August 2001; **Revised** 17 May 2002; **Accepted** 25 January 2003; **Published** 22 April 2003.

Tackley, P. J., and S. D. King, Testing the tracer ratio method for modeling active compositional fields in mantle convection simulations, *Geochem. Geophys. Geosyst.*, *4*(4), 8302, doi:10.1029/2001GC000214, 2003.

Theme: Thermochemical Convention in the Earth's Interior
Guest Editors: Peter van Keken, Louis Moresi, and Adrian Lenardic

1. Introduction

[2] Chemical variations are important in Earth's mantle and thus, methods for accurately treating them in numerical models of mantle convection are of great interest to the modeling community. Chemical fields are much more challenging to model than the temperature field because the chemical diffusivity is effectively zero, thus the appropriate differential equation has a hyperbolic, as opposed to parabolic, form and different numerical methods are required.

[3] Several techniques have been used to represent active chemical fields in numerical simulations, some representative implementations of which were compared and benchmarked in *van Keken et al.* [1997]. Continuum field techniques are straightforward but require very small grid spacing in order to make numerical diffusion small enough for long term integrations [e.g., *Ogawa*, 2000; *Ten et al.*, 1997]. Marker chains are useful for treating simple sharp boundaries but become unfeasible once entrainment and stirring make the boundary topologically complex [*van Keken et al.*, 1997]. Tracer particle methods have great potential, with (neglecting errors in position due to advection error) zero diffusion, and the possibility of resolving features narrower than the grid spacing. However, problems arise when converting a distribution of tracers to its equivalent continuum field, mainly because of the statistical variation in tracer density (i.e., number of tracers per unit volume) from place to place [*Christensen and Hofmann*, 1994], which can cause spurious variations in density, resulting in settling of tracers and unphysical features in the resulting flows.

[4] In the broader numerical modeling community, particles are often used to advect most or all fields, including temperature, momentum, and magnetic field [e.g., *Brackbill*, 1991; *Monaghan*, 1985; *Munz et al.*, 1999; *Sulsky et al.*, 1995]. The general approach, known as particle in cell (PIC), combines Eulerian grid based velocity calculation with Lagrangian particle based advection. This involves interpolation at each time step between field values defined at grid points and field values carried by particles. In the mantle dynamics community, particle methods have thus far been restricted to compositional fields, and two basic methods have been used for representing a continuum field C, here assumed to vary between 0 and 1, with a distribution of tracers. In the most commonly used method, here referred to the "absolute" method, tracers represent the $C = 1$ component, lack of tracers indicates $C = 0$ and hence the local value of C (hence density) is proportional to the absolute local tracer density. It is necessary to have several tens of tracers per cell to get acceptably small statistical variations in C from cell to cell [*Christensen and Hofmann*, 1994; *van Keken et al.*, 1997]. In the second, "ratio" method, which has its roots in [*Harlow and Welch*, 1965], one type of tracer represents the $C = 1$ component while another type of tracer represents the $C = 0$ component, with C being equal to the local fraction of $C = 1$ tracers (i.e., the ratio of $C = 1$ tracers to total tracers). This ratio method has reportedly been found (W.-S. Yang, personal communication, 1999; H. Schmeling, indirect personal communication, 2001, T. Nakakuki, indirect personal communication, 2001) to require much fewer tracers per cell than the absolute method, at least for simulating the long term evolution of a stable layer, a problem that has received a lot of recent interest [*Hansen and Yuen*, 2000; *Kellogg et al.*, 1999; *Tackley*, 1998, 2002]. However, this claimed advantage has not been rigorously documented, at least in the mantle convection community.

[5] The purpose of this paper is to document the performance of the ratio method by first verifying its validity using standard benchmarks, then comparing the performance of the "absolute" and "ratio" tracer methods for modeling the long term evolution of a convecting system with a deep, dense layer. The performance of both tracer methods is also compared to that of two commonly used grid-based advection schemes.

2. Numerical Methodology

[6] The equations solved are those of infinite-Prandtl number, constant viscosity Boussinesq

convection between isothermal, free-slip horizontal boundaries.

$$\nabla \bullet \vec{v} = 0 \tag{1}$$

$$\nabla \bullet \left[\eta\left(\nabla\vec{v} + (\nabla\vec{v})^T\right)\right] - \vec{\nabla}p = Ra.(T + BC)\hat{\vec{z}} \tag{2}$$

$$\frac{\partial T}{\partial t} + \vec{v} \bullet \vec{\nabla}T = \nabla^2 T \tag{3}$$

$$\frac{\partial C}{\partial t} + \vec{v} \bullet \vec{\nabla}C = \frac{1}{Le}\nabla^2 C \tag{4}$$

where $\vec{v}$, p, T and C are variables velocity, pressure, temperature and composition respectively, $\hat{\vec{z}}$ is a vertical unit vector (positive up), Ra is the Rayleigh number, B is the chemical buoyancy ratio, and Le is the Lewis number, which is the ratio of thermal diffusivity to chemical diffusivity. The desired limit is that of infinite Le (i.e., $1/Le = 0$, zero chemical diffusion), but for numerical reasons a finite Le is often assumed.

[7] Test results are computed using two completely different codes for calculating the flow field and time stepping scalar fields. The codes are Stag3D [*Tackley*, 1998, 1996], which uses a finite volume multigrid method based on staggered grid primitive variables, and ConMan [*King et al.*, 1990], a widely used finite element code that uses bilinear shape functions for velocity (and constant pressure).

2.1. Advection of Grid-Based Fields

[8] The two codes use different methods for advecting temperature; these methods are also used for advecting composition in some tests. Stag3D uses MPDATA [*Smolarkiewicz*, 1984], which is based on the upwind donor cell scheme and iteratively corrects for numerical diffusion to achieve second order accuracy. Six iterations are used for the tests reported here, as fewer resulted in significantly greater numerical diffusion. ConMan uses Petrov-Galerkin upwinding that is second order in space and a predictor-corrector method that is second order in time; further details can be found in *van Keken et al.* [1997]. Also implemented in both codes is the filtering scheme by *Lenardic and Kaula* [1993], which is designed to maintain sharp material interfaces, and is therefore only used for the compositional field.

2.2. Tracer Advection

[9] In both codes, tracers are advected using a 4th order Runge-Kutta scheme, with spatial interpolation of velocities performed using bilinear shape functions in ConMan, but second-order interplation in Stag3D. The accuracy of tracer advection has been verified using a standard test reported in *van Keken et al.* [1997], in which a tracer is advected for one circuit in a steady velocity field; the error in tracer position is of order 10^{-5}. Tracers are initialized on a regular grid with each tracer perturbed from its grid position by a random amount of up to ±half a grid spacing, in order to eliminate artifacts due to tracer alignment.

2.3. Converting Tracer Distributions to *C*

[10] In order to calculate the velocity/pressure solution at each time step, the buoyancy associated with the composition field must be calculated at the appropriate grid points, which are different for the two flow solvers. ConMan requires buoyancy at the nodes, which are at the corners of the elements. Stag3D requires buoyancy at the same positions as vertical (z) velocity, i.e., in the center of the cell faces perpendicular to the z-direction. Because chemical buoyancy is proportional to C (equation (2)), we here discuss the calculation of C.

2.3.1. Integrating Over the Local Tracers

[11] Calculation of C at a particular point requires integrating over the tracer distribution in the surrounding region, most logically defined using conventional finite element shape functions. Each tracer is treated as a delta function. Thus the (generally noninteger) number of tracers in the surrounding region is given by:

$$N_i = \int_{domain} S_i(\vec{x}) \sum_{j=1}^{Ntr} \delta(\vec{x} - \vec{x}_j) dV = \sum_{j=1}^{Ntr} S_i(\vec{x}_j) \tag{5}$$

where S_i is the shape function for point i, and $\vec{x}_j$ are the positions of the tracers. (Because S_i are

localized, it makes no difference whether the integration limits are the entire domain or just the local region for which $S_i \neq 0$.) The volume of the local region is:

$$V_i = \int_{domain} S_i(\vec{x}) dV \quad (6)$$

These equations apply to finite elements or volumes of arbitrary shape or size, although the cases presented here use only rectangular grids with uniform spacing. In ConMan, the shape functions S_i are the same bilinear nodal shape functions used in the solution of the velocity equation. In Stag3D, the underlying solver does not utilize shape functions so different choices can be made and two are tested: bilinear functions identical to those used in ConMan, and constant or "cell" functions, which are 1.0 in the cell surrounding the grid point (i.e., extending halfway to adjacent grid points) and zero elsewhere. For an evenly-space two-dimensional rectangular grid with spacing Δx and Δz in the x- and z-directions respectively, the bilinear shape function for node i at position (x_i, z_i) is given by:

$$S_i(x,z) = \max\left(0, 1 - \frac{|x - x_i|}{\Delta x}\right) \max\left(0, 1 - \frac{|z - z_i|}{\Delta z}\right) \quad (7)$$

whereas the constant (cell) shape function is given by:

$$S_i(x,z) = H(\Delta x/2 - |x - x_i|) H(\Delta z/2 - |z - z_i|), \quad (8)$$

where $H(x)$ is the Heaviside step function. For non-rectangular or irregular grids the reader is referred to standard finite element texts [e.g., *Hughes*, 2000; *Zienkiewicz and Taylor*, 2000] for the relevant forms.

[12] The integration in (5) can be thought of as a local averaging of the tracer distribution in the region around each buoyancy point. Since velocity and other grid-based fields cannot be resolved at a smaller scale than the grid spacing, this is the minimum possible scale at which this averaging can be performed, as well the logical scale considering the points at which buoyancy must be calculated. If a more localized integration function was used then some tracers would be missed, while a broader integration function would smear the field. The bilinear shape function integrates/averages over a larger region than the constant/cell function (4 times larger in 2-D, 8 times larger in 3-D).

[13] The integration over tracer delta functions may alternatively be viewed as a partitioning of each tracer's contribution between nearby points. With the constant/cell shape function, 100% of a tracer's contribution is assigned to the closest point, resulting in a discontinuous change in the calculated C value as a tracer moves from one cell to the next. In contrast, with the bilinear function each tracer's contribution is partitioned between the four (in 2-D) or eight (in 3-D) nearest points, resulting in smooth changes in C as a tracer moves around, and giving better physical fidelity because the nodes "see" the tracer at the correct position.

2.3.2. Absolute Method

[14] In the absolute method, C is proportional to the local tracer density, i.e., number of tracers per unit volume:

$$C_i = A \frac{N_i}{V_i} \quad (9)$$

where A is a constant equal to the initial volume of the dense layer divided by the number of tracers representing the dense layer. Each tracer effectively carries a mass anomaly that remains fixed throughout the calculation, guaranteeing conservation of mass. However, C can become unphysically significantly greater than 1 due to statistical fluctuations in N_i or clumping or settling of tracers. Truncating C values at 1 may help (P.E. van Keken, personal communication, 2001), but mass conservation is then violated.

2.3.3. Ratio Method

[15] In the ratio method, C is proportional to the ratio of dense tracers to total number of tracers in the region around each point:

$$C_i = \frac{N_i^{dense}}{N_i^{dense} + N_i^{regular}} \quad (10)$$

Thus, C cannot become larger than 1. Mass conservation is, however, not guaranteed for this

method, although it should occur on average. An alternative way of viewing this, which is useful for extension to smoothly-varying fields, is that tracers carry a C value of 0 or 1 (the value of C at their initial position), and C at a grid point is the local average of C^{tr} carried by the nearby tracers, i.e.,

$$C_i = \frac{1}{N_i} \int_{domain} S_i(\vec{x}) \sum_{j=1}^{Ntr} C_j^{tr} \delta(\vec{x} - \vec{x}_j) .dV = \frac{1}{N_i} \sum_{j=1}^{Ntr} C_j^{tr} S_i(\vec{x}_j) \quad (11)$$

[16] In ConMan, C hence chemical buoyancy is calculated at the nodes. In Stag3D, C is first calculated at the cell centers, which is where scalar fields T, p, η etc. are defined in the finite volume method, then interpolated to the buoyancy points. In principle C could be calculated directly at buoyancy points, something that should be tested in future.

2.4. Standard Benchmarks

[17] The ratio method is first tested using Stag3D (using bilinear shape functions) against the two-dimensional benchmark tests detailed in *van Keken et al.* [1997], who presented results for several different codes and numerical techniques. In the cases where viscosity is dependent on C, the viscosity is calculated at cell centers assuming a linear variation with C.

2.4.1. Rayleigh-Taylor Overturn of a Buoyant Layer

[18] This test treats the Rayleigh-Taylor instability of a buoyant layer with no thermal effects. The buoyant material has either the same viscosity, 1/10th the viscosity, or 1/100th the viscosity of the (initially) overlying material.

[19] This benchmark was here performed with grid resolutions of 64 × 64 or 128 × 128 and with either 5, 15, or 40 tracers per cell (on average). Images of the C field at a time of 1500 for all six permutations and three viscosity contrasts are presented (Figure 1, compare with Figures 2, 4 and 6 in *van Keken et al.* [1997]), and sample time series for each case are given in Figure 2 (compare to Figures 3, 5 and 7 in *van Keken et al.* [1997]). The requested quantitative diagnostics growth rate (at time = 0), maximum v_{rms} and the time at which it occurs, are listed in Table 1.

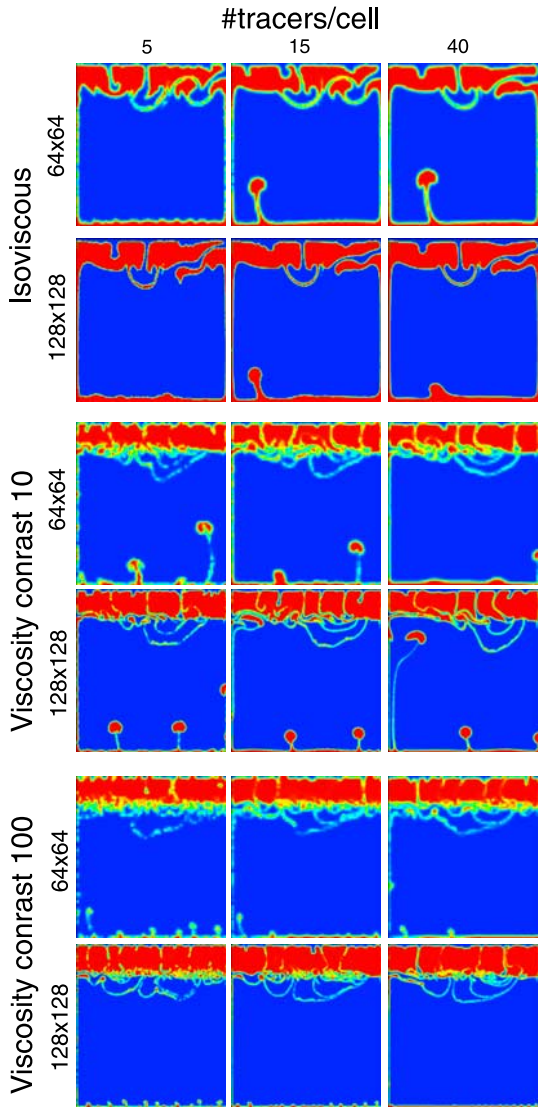

Figure 1. Compositional fields for the Rayleigh-Taylor benchmark using the ratio method at a nondimensional time of 1500. (top 2 rows) The isoviscous case, (middle 2 rows) viscosity contrast $\Delta\eta$ = 10, (bottom 2 rows) $\Delta\eta$ = 100. (left column) 5 tracers/cell, (center column) 15 tracers/cell, (right column) 40 tracers/cell. C varies from 0 (blue) to 1 (red).

2.4.1.1. Constant Viscosity

[20] For the constant viscosity case, results that are similar to the published results are obtained on the 64 × 64 grid with 40 tracers/cell or on the 128 × 128 grid with 15 or 40 tracers/cell. With 5 tracers/cell there are noticable differences, and with the 64

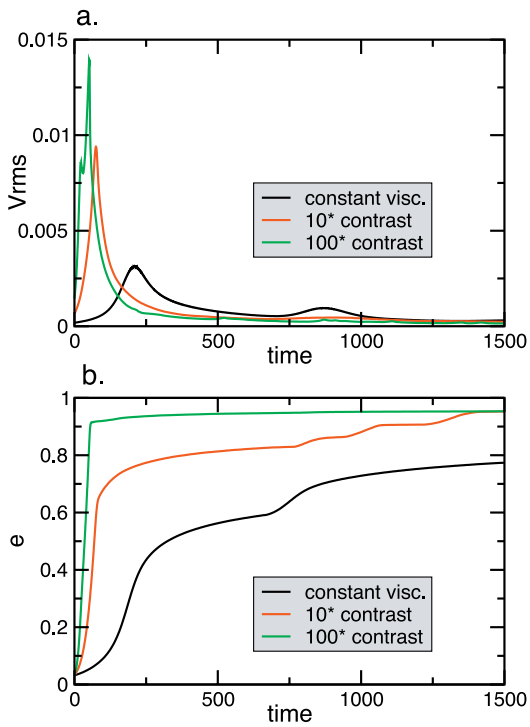

Figure 2. Time series of rms. velocity and entrainment for the Rayleigh-Taylor benchmark with the three viscosity contrasts. The cases are constant viscosity with a 64 × 64 grid and 40 tracers/cell, $\Delta\eta = 10$ with a 128 × 128 and 15 tracers/cell, and $\Delta\eta = 100$ with a 128 × 128 and 40 tracers/cell.

× 64 grid and 5 or 15 tracers/cell a downwelling instability in the upper right that was seen in *van Keken et al.* [1997] to occur between $t = 1500$ and $t = 2000$, has occurred before $t = 1500$. Time series of rms. velocity and entrainment for the 64 × 64, 40 tracers/cell case (Figure 2) are similar to those in the benchmark paper. Quantitative diagnostics are consistent with published results.

2.4.1.2. Viscosity Contrast 10

[21] There were significant differences between the various results illustrated in *van Keken et al.* [1997]. The present cases with 40 tracers/cell or grid resolution of 128 × 128 and 15 tracers/cell are within the published range of variation. All cases all have a similar character but differ in details, with fewer tracers/cell leading to more small-scale instabilities due to tracer discretization noise. On the 64 × 64 grid fine-scale features appear blurred in the plot, because the size of the smallest features is less than the grid scale. Quantitative diagnostics are consistent with published results.

2.4.1.3. Viscosity Contrast 100

[22] The results published in *van Keken et al.* [1997] are substantially different from each other in small-scale details, such that a wider range of the present results may appear to be acceptable. Again, a 128 × 128 grid yields better results, and fewer tracers/cell gives more noise. With the 64 × 64 grid the peak velocity occurs a bit later than published results.

[23] Other numerical details made subtle differences to the results, including the method of calculating viscosity for compositions between 0 and 1 and the time step: smaller steps gave peak diagnostics (maximum velocity and associated time) closer to the benchmark solutions.

[24] The conclusion from these results is that having grid resolution sufficient to resolve small-scale active features is important, as is required when using a continuum field approach. If that condition is met, which may require a 128 × 128 grid in some cases, reasonable result can be obtained with

Table 1. Selected Quantities for the Rayleigh-Taylor Problem

Grid	#tr	Growth rate	t(max v_{rms})	max v_{rms}
		Isoviscous		
64^2	5	0.01112	206.5	0.003041
	15	0.01117	208.8	0.003098
	40	0.01115	209.9	0.003110
128^2	5	0.01113	208.1	0.003079
	15	0.01110	208.9	0.003097
	40	0.01109	209.2	0.003102
		$\Delta\eta = 10$		
64^2	5	0.04388	72.4	0.009169
	15	0.04539	73.0	0.009226
	40	0.04530	73.5	0.009285
128^2	5	0.04510	72.8	0.009407
	15	0.04530	73.0	0.009380
	40	0.04516	73.0	0.009383
		$\Delta\eta = 100$		
64^2	5	0.09858	53.6	0.01185
	15	0.1034	53.5	0.01204
	40	0.1007	53.5	0.01213
128^2	5	0.0994	51.1	0.01345
	15	0.1013	51.0	0.01399
	40	0.1013	51.0	0.01398

few tracers per cell, although better, less noisy results are obtained with more tracers/cell.

2.4.2. Entrainment of a Thin Layer

[25] This test models the entrainment of a thin (0.025), dense layer by thermal convection in an aspect ratio 2 box at a Rayleigh number of 3×10^5. The ratio method is rather inefficient here because 40 times as many tracers are required than would be for the absolute method with the same number of tracers/cell.

[26] Here the ratio technique is tested, with a grid resolution of 64 in the vertical direction and either 64 or 128 in the horizontal direction, and 5, 15 or 40 tracers per cell. A typical case, using a 64×64 grid with 15 tracers per cell is illustrated in Figure 3. The evolution of the C field is consistent with the results shown in Figures 8–11 of *van Keken et al.* [1997], which diverge from each other.

[27] Entrainment curves during the first part of the simulation are illustrated in Figure 4 (compare to the inset in Figure 12b in *van Keken et al.* [1997]). The curves have a similar shape to those previously reported, with an absolute amplitude that depends on numerical details. Tracer discretization is noticable particularly with fewer tracers/cell. On a 128×64 grid entrainment at time = 0.02 ranges from 0.06–0.067 depending on #tracers/cell, consistent with the previously reported results. With the coarser grid, e(0.02) ranges from 0.072 to 0.093, perhaps a little high but still within the previously reported range. Test using the absolute method in Stag3D [*Tackley*, 1998] obtained slightly higher entrainment for the same grids.

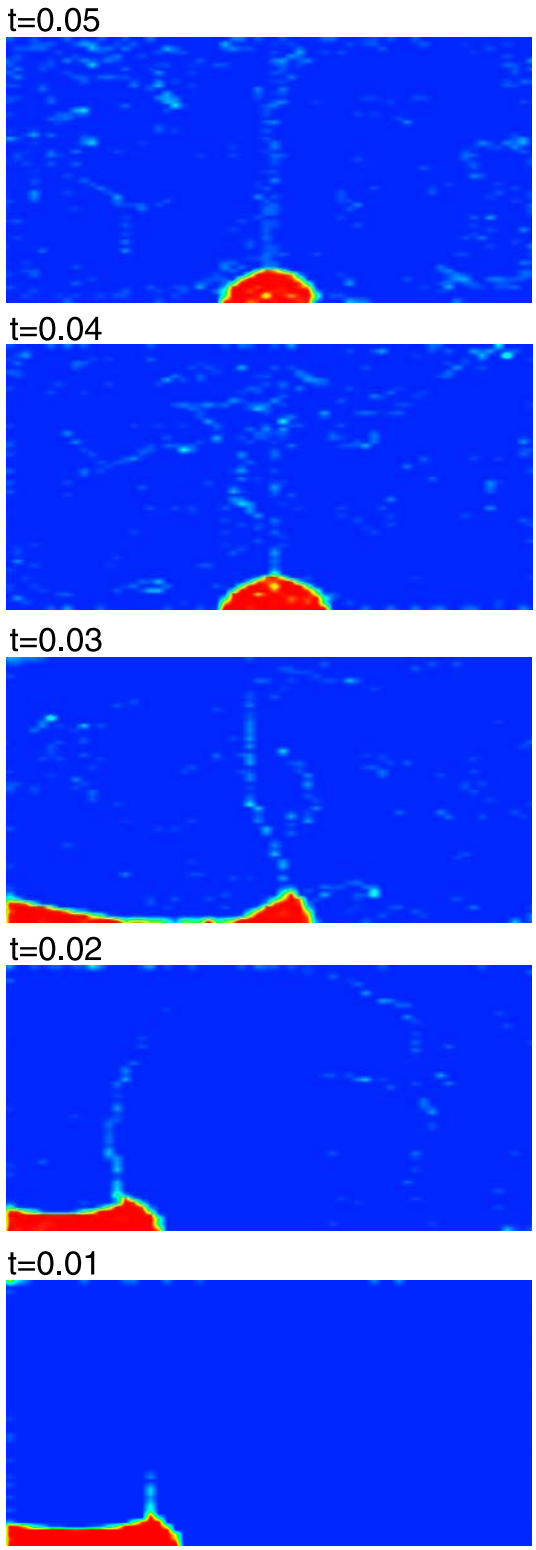

Figure 3. Evolution of the C field for the thin layer entrainment benchmark run with 64×64 grid points and 15 tracers per cell. Times vary between 0.01 and 0.05 as indicated. *C* varies from 0 (blue) to 1 (red).

3. Long Time, Thick Layer Test

3.1. Definition

[28] A new benchmark test is presented based on simulating the long-term evolution of a deep, dense, stable layer in a convecting mantle. The focus is on 2-D with a few 3-D results. A Boussinesq, constant physical properties fluid is assumed in a 1×1 box ($1 \times 1 \times 1$ in 3-D) with reflecting side boundaries and free-slip, isothermal, horizontal boundaries. The thermal Rayleigh number is

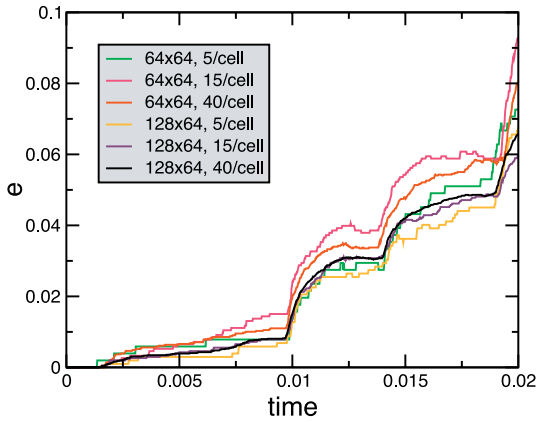

Figure 4. Entrainment versus time up to a time of 0.02 for the thin layer entrainment benchmark with six combinations of grid resolution and tracers/cell as indicated.

10^6. The chemical buoyancy ratio B is -1.0. C is initially a flat layer occupying the lower 40% of the box. T is initialized from a steady state thermal convection solution (Figure 5).

[29] The model is integrated for a time of 0.1, which typically takes several thousands of time steps, and may scale to billions of years. With these parameters, convection occurs in both layers, with an overall Nusselt number of ~7 (compared to ~20 for unlayered cases). For the final state, visual comparisons of thermal and chemical fields are made, plus quantitative diagnostics (1) C_{max}, the maximum value of the C field, (2) the fractional error in the volume integral of C ("C mass error"), given by

$$\Delta M_C = \frac{(\int C) - (\int C)_{initial}}{(\int C)_{initial}} \quad (12)$$

where the integration is over the entire domain, and (3) the fraction of dense material entrained above a depth of 0.5, given by

$$e = \frac{1}{0.4} \int_{0.5}^{1} \int_{0}^{1} C dx dz. \quad (13)$$

3.2. Results

[30] Results are presented and compared for both tracer field (absolute, truncated absolute and ratio) and grid-based field (with or without the "Lenardic" filter) approaches using both ConMan and Stag3D. For the tracer methods, bilinear shape functions are used for all cases, with constant/cell shape functions additionally tested using Stag3D. The average number of tracers per cell is varied from 5 to 160, although the actual number can vary substantially from this mean. 2.5 times as many tracers are needed in the ratio method as in the absolute method.

3.2.1. Tracer Methods

[31] Remarkably similar results are obtained with the two different codes Stag3D and ConMan. The T and C fields for these are shown in Figures 6 and 7 respectively, with quantitative diagnostics compared in Figure 8.

[32] The absolute method suffers from dramatic tracer settling for #tracers/cell<40 (Figures 6–7), resulting in maximum C values very much higher than 1.0 (Figure 8a). This settling results in a reduced, stably stratified layer that does not internally convect. C_{max} values (Figure 8a) indicate that constant shape functions give greater settling than bilinear shape functions for Stag3D, although ConMan appears to experience greater settling

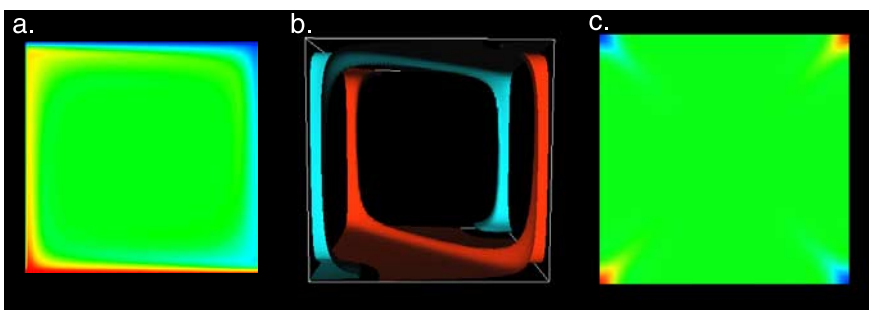

Figure 5. Initial steady state temperature fields for the deep stable layer test. (a) in two dimensions, (b) in three-dimensions, isosurfaces of (blue) $T = 0.25$ and (red) $T = 0.75$, and (c) 3-D, mid-depth temperature cross-section. The 3-D solution can be obtained by initializing with $T = 0.5 + 0.1 \sin(\pi z) \cos(2\pi x) \cos(2\pi y)$ and running to steady state.

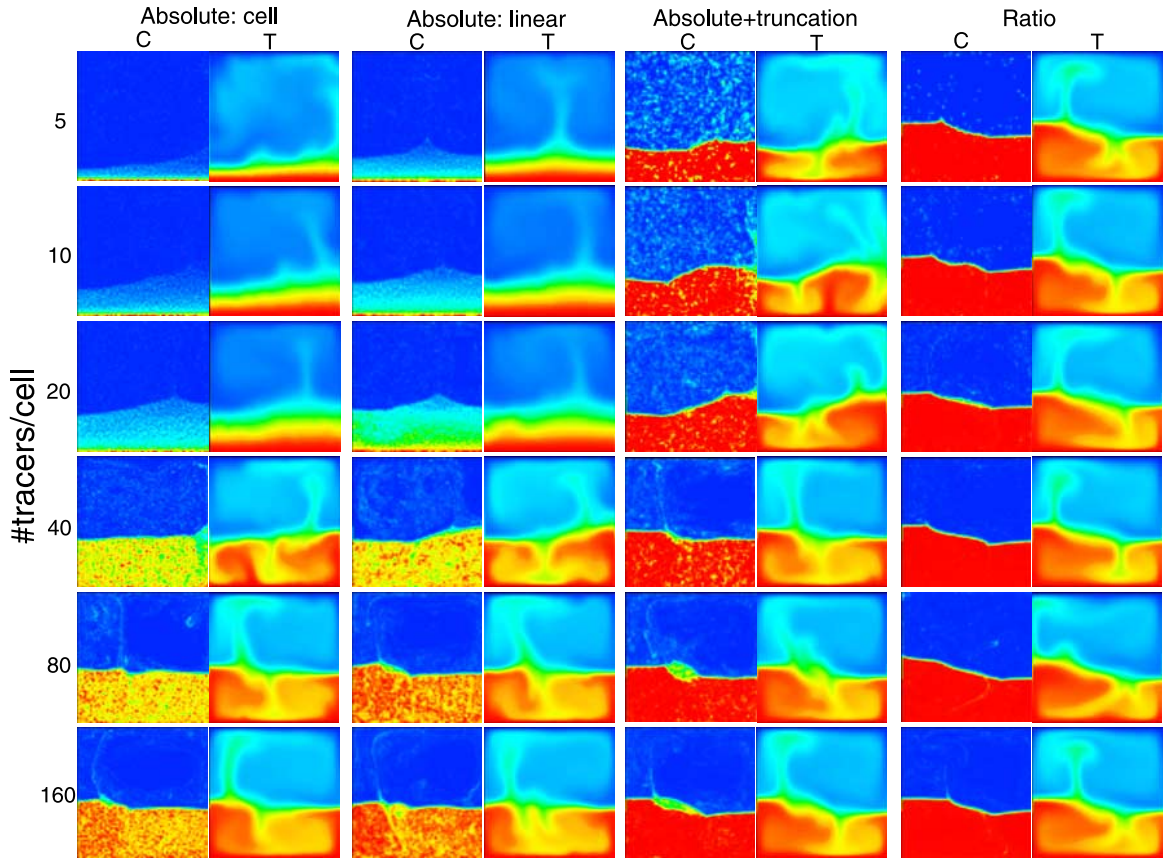

Figure 6. *C* and *T* fields for Stag3D tracer advection tests at a time of 0.1 for (columns, as labeled) different methods and (rows, as labeled) tracers/cell varying from 5 to 160. The color scheme is scaled from 0 to the maximum value in each frame, which is 1.0 for *T* and for *C* in ratio or truncated cases, but >1 for *C* in absolute non-truncated cases as given in Figure 8a.

even using bilinear shape functions, perhaps because the order of velocity interpolation during tracer advection is lower. For $\geq$40 tracers/cell settling is not observed but the *C* field is very noisy, with $C_{max} > 1.17$ for both codes even with 160 tracers/cell. Truncating *C* at 1.0 provides a great improvement, eliminating settling and reducing noise, although substantial entrainment and layer shrinkage is visible with <40 tracers/cell.

[33] Using the ratio method, *C* and *T* fields using 5 tracers/cell appear similar to those with 160 tracers/cell. There is no noticable settling and little noise, and low entrainment. Ratio method solutions are similar to the truncated absolute solution with 80–160 tracers/cell (these solutions are slightly time-dependent).

[34] C mass error is substantial when truncation is added to the absolute method (Figure 8b)- between 0.775% (160 tracers/cell; ConMan) and 16.4% (5 tracers/cell; Stag3D). With the ratio method, this is always less than 0.65% using linear shape functions.

[35] Entrainment displays different trends with increasing #tracers/cell, depending on the method (Figure 8c). For the absolute method entrainment decreases whereas for the ratio method it increases, and is much smaller. Truncation greatly increases entrainment with few tracers/cell. Entrainment converges with increasing tracers/cell, although it has not fully converged even with 160 tracers/cell. It appears that ConMan results converge to an asymptotic value more rapidly than Stag3D results, particularly for the ratio method where little change in entrainment is observed between 10 and 160 tracers/cell.

[36] It is not clear from logical reasoning how the required number of tracers per cell scales from 2-D

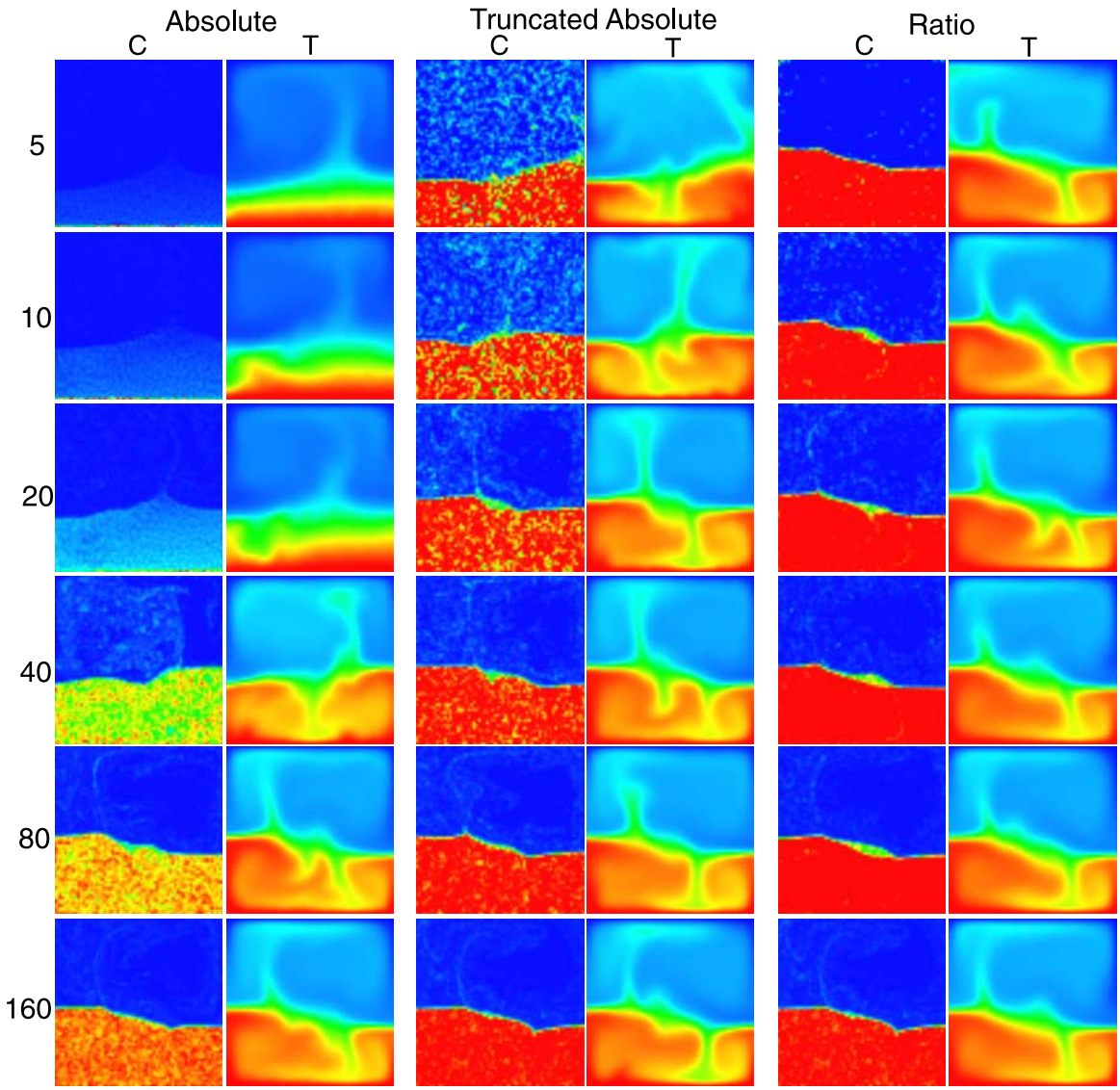

Figure 7. *C* and *T* fields for ConMan tracer advection tests at a time of 0.1 for (columns, as labeled) different methods and (rows, as labeled) tracers/cell varying from 5 to 160. The color scheme is scaled from 0 to the maximum value in each frame, which is 1.0 for *T* and for *C* in ratio or truncated cases, but >1 for *C* in absolute non-truncated cases as given in Figure 8a.

to 3-D. From a statistical viewpoint (i.e., considering the random fractional variation in tracers/cell, which for a Poisson distribution scales as $1/\sqrt{}$(tracers/cell)), the requirement is independent of dimensionality. Alternatively, to resolve small-scale features, the average spacing between adjacent tracers may be key, leading to tracers/cell scaling as the power of dimensionality, i.e., $N_{3D} = N_{2D}^{3/2}$. These are limiting cases.

[37] Four 3-D cases have been run using Stag3D, the ratio method with linear shape functions and 5 to 40 tracers/cell. *T* and *C* fields (Figure 9) indicate long-term stable layering with a sharp boundary even with only 5 tracers/cell. The fields evolved slowly, initially following the same path with upwellings and downwellings in the corners where they started. However, mechanical coupling is preferred over thermal coupling for constant viscosity, so some upwellings and downwelling moved, at which point the solutions became slightly different. Cross-sections of *C* reveal a sharp boundary and more entrainment than in 2-D as confirmed quantitatively (Figure 8c), although since the physically correct

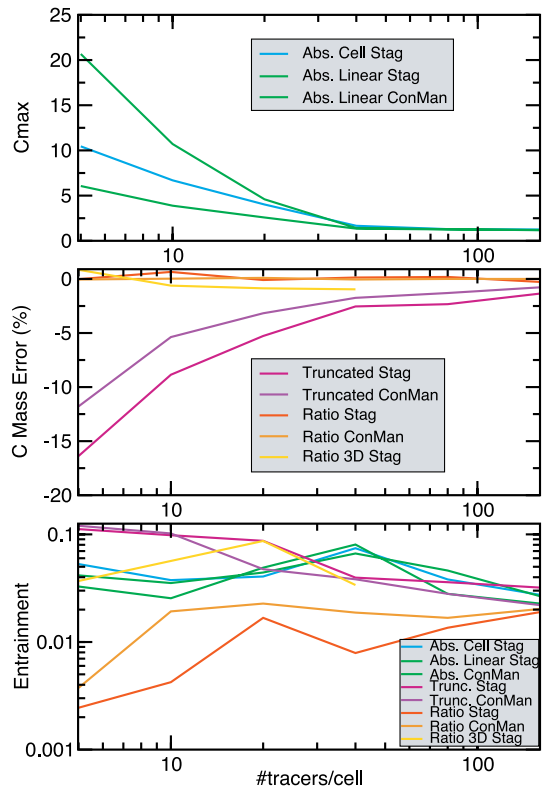

Figure 8. Scaling of (top) maximum C value, (center) C mass error, and (bottom) entrainment as a function of #tracers/cell, for Conman and Stag3D tracer methods as indicated in legends.

entrainment is likely different in 3-D than in 2-D, such a comparison may not give useful information about the numerical scheme. C mass error (Figure 8b) appears slightly larger than in 2-D but still less than 1%.

3.2.2. Grid Methods

[38] Results were computed with ConMan for $1/Le$ between 10^{-2} and 10^{-5} and grid resolutions of 64 $\times$ 64 or 128 $\times$ 128, and for Stag3D with no added diffusion (i.e., numerical diffusion only) and 64 $\times$ 64, 128 $\times$ 128, or 256 $\times$ 256 cells. All advection methods used conserve mass (i.e., C mass error is zero) and produce only small overshoots (i.e., C_{max} is always less than 1.05), so the discussion here focuses on entrainment. Although stable layers survive in all cases, it is apparent both visually (Figure 10) and quantitatively (Figure 11) that for the basic (unfiltered) advection techniques entrainment is an order of magnitude higher than for converged tracer methods. Adding the Lenardic filter greatly reduces entrainment, to less than tracer methods in some cases. In the ConMan and and 256 $\times$ 256 Stag3D calculations, adding the Lenardic filter changes the pattern of the flow. The fields from the grid method with the filter are consistent with the tracer-based fields.

[39] Numerical diffusion in ConMan can be estimated from the graph of entrainment versus 1/Le (Figure 11a)- once 1/Le is less than numerical diffusion, entrainment should stop changing. Cases with no filter display little change in entrainment with 1/Le, suggesting that numerical diffusion is greater than 10^{-2} times thermal diffusion. The filtered results suggest that the effective numerical diffusion coefficient is in the range 10^{-4}–10^{-5}.

[40] Increasing grid resolution reduces entrainment, and it appears that an asymptotic value has not been reached at the maximum resolutions used here (128 $\times$ 128 for Conman or 256 $\times$ 256 for Stag3D). Stag3D displays significantly more entrainment than ConMan, which could be due to a combination of two reasons: (1) MPDATA, the advection method used in Stag3D, is known to be diffusive relative to other finite volume advection schemes [*Muller*, 1992], some of which are specifically designed for advecting sharp features such as discontinuities. (2) The points at which buoyancy must be known are vertically mid-way between the points at which scalar fields C and T are defined; the resulting interpolation vertically smears the fields, as far as the flow solver is concerned.

[41] Regarding visual patterns (Figure 10), none of the unfiltered cases reproduce the solution obtained with tracers; the Lenardic filter is required, and (particularly for Stag3D), higher resolution.

3.2.3. Execution Time

[42] The tracer-based methods take considerably longer to run than grid-based methods; indeed, advecting tracers takes the majority of execution time. Examples are given for Stag3D running on a 400 Mhz Pentium II Linux PC. A very efficient stream function-based flow solver is used for constant viscosity cases. Grid based field cases take 0.155 s/step on a 64 $\times$ 64 grid and 0.65 s/step on a

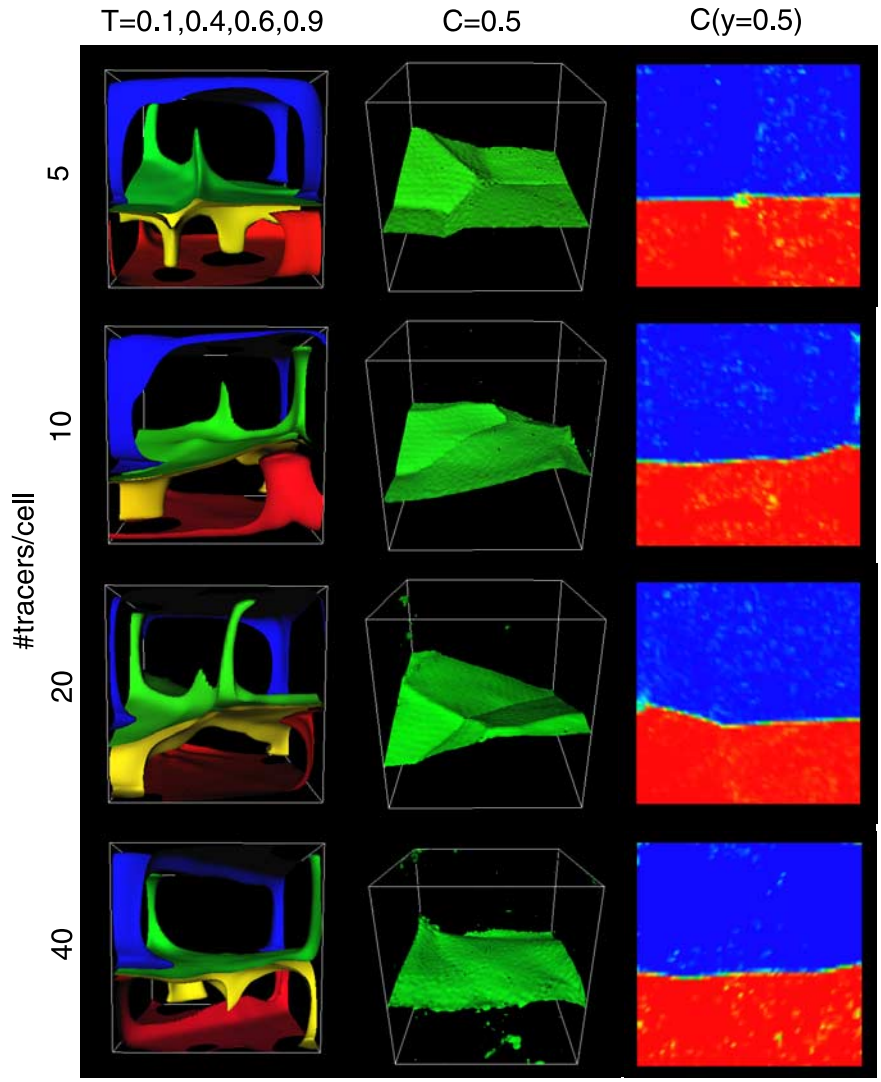

Figure 9. 3-D cases at a time of 0.1 using the ratio method with (rows, as indicated) between 5 and 40 tracers/cell. (left column) T isosurfaces 0.1 (blue), 0.4 (green), 0.6 (yellow) and 0.9 (red); (center column) isosurface $C = 0.5$, and (right column) vertical slice through the C field at $y = 0.5$.

128×128 grid, faster than the ratio method on a 64×64 grid, which varies linearly with #tracers between 0.82 s/step (5 tracers/cell) and 23.8 s/step (160 tracers/cell). Such differences in execution time must be considered when deciding which method to use.

4. Discussion

[43] It is useful to compare the tracer ratio method and the filter by *Lenardic and Kaula* [1993], because both tend to sharpen material interfaces. There is a fundamental difference in that the Lenardic filter causes irreversible long-range interactions at each timestep in order to enforce conservation: any net loss or gain of material caused by localized truncation of advection overshoots is compensated for by a correction spread over the entire domain. In contrast, the tracer ratio method does not involve moving any tracers or permanently changing their values. It is simply a method of converting a given tracer distribution to a grid-based field in a manner that tends to produce regions with uniform values separated by sharp interfaces.

[44] Entrainment rates are important to quantify in order to constrain Earth's thermo-chemical evolution. The differences in entrainment rates between different methods and even between the same

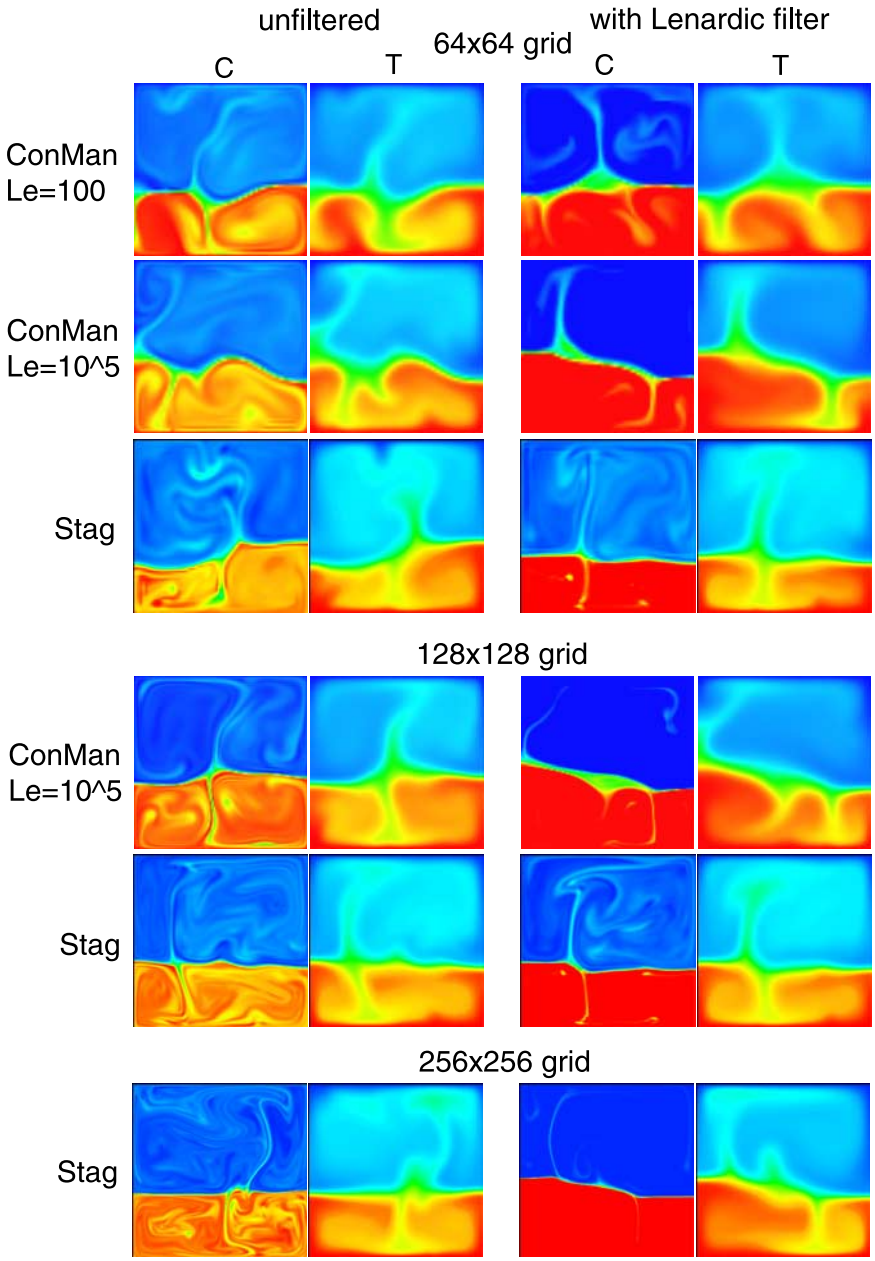

Figure 10. *C* and *T* fields for grid-based advection tests using Conman and Stag3D at a time of 0.1. Cases on the left use the basic advection methods, whereas cases on the right additionally use the Lenardic filter.

method with different grid resolutions, is thus a serious problem. Tracer methods appear to be on a convergent path as the number of tracers is increased, at least for the grid resolution considered here, and the discrepancies between absolute and ratio methods with few tracers/cell are easy to understand, at least qualitatively. The ratio method underestimates entrainment because with few tracers/cell the buoyancy represented by a single entrained dense tracer is quite large, making it difficult to entrain. The absolute method overestimates entrainment with few tracers/cell because tracer settling reduces the density contrast at the top of the dense layer, making it easier to entrain. The large entrainment obtained with non-filtered grid-based advection methods is also easy to understand: grid-based methods suffer numerical diffusion, which smears density interfaces over several grid spacings; the less dense material from the top of the smeared interface is easy to

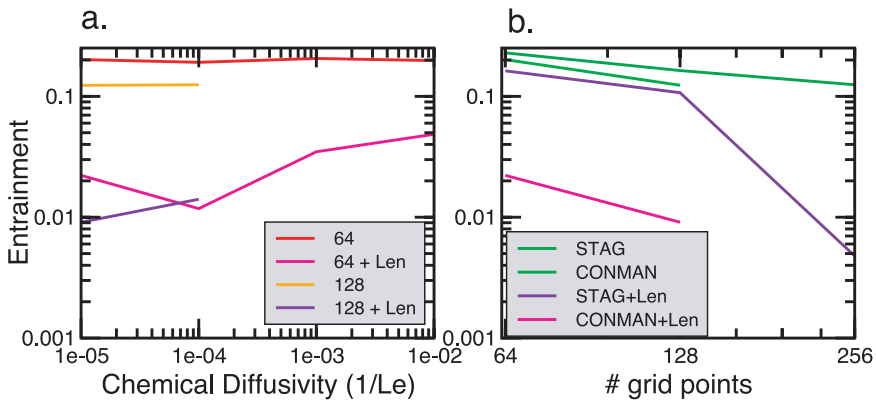

Figure 11. Effect of numerical parameters on entrainment for grid-based advection tests. (a) ConMan with varying chemical diffusivity (1/Le), (b) Stag3D and ConMan with varying grid resolutions, 64 × 64, 128 × 128, or 256 × 256 elements or cells.

entrain. The Lenardic filter strongly reduces this smearing.

[45] However, while tracer methods appear to be a convergent path as #tracers is increased, it is not clear that grid-based methods are converging with decreasing grid spacing, and there is a quantitative discrepancy between tracer-based and grid-based methods in the present tests. Convergence must be tested by going to much higher resolutions with all techniques, and numerical results must be tested against entrainment rates determined in laboratory experiments [*Davaille*, 1999a, 1999b].

[46] A possible improvement Stag3D's tracer field treatment is to calculate C directly at the buoyancy points using (5)–(10), rather than, as is presently done to be consistent with the finite volume staggered grid definition, calculating C at cell centers then interpolating to the buoyancy points, a step that makes the flow solver "see" a slightly smeared-out version of the C field, possibly increasing entrainment.

5. Conclusions and Future Directions

[47] For the Rayleigh-Taylor overturn of an unstable layer or the (relatively) rapid entrainment of a thin layer [*van Keken et al.*, 1997], the ratio method obtains correct results if the grid spacing is small enough to resolve dynamically important features and there are enough tracers per cell to reduce noise acceptably. For these cases, however, it does not appear to offer a clear advantage over the methods reported in *van Keken et al.* [1997]. The Rayleigh-Taylor benchmark may be more susceptible to discretization noise than the new, stable layer test because with an unstable layer, positive feedback, rather than negative feedback as with a stable layer, operates on any numerical perturbations to the layer boundary. For simulating a very thin layer, the ratio method is inefficient because tracers must be placed everywhere instead of only in the layer.

[48] In contrast, for the long-term integration of convection with a thick stable layer, the tracer ratio method has several advantages over the absolute tracer method, obtaining even with ~5 tracers/cell: (1) no C values greater than 1, (2) minimal variations of C within the dense layer, (3) sharp, stable layering, and (4) low entrainment rates (perhaps unrealistically so for few tracers/cell). The choice of method should thus be made according to the physical situation being modeled.The advection of tracers and projection of tracers to grid points is computationally burdensome. This makes the ratio method attractive because the number of tracers per cell can be reduced.

[49] The grid-based advection methods tested here experience an order of magnitude greater entrainment than tracer-based methods unless an interface-sharpening filter is applied [*Lenardic and Kaula*, 1993]. Even then, entrainment rates are highly resolution-dependent, and higher grid resolution may be required to obtain the same solution obtained with tracer methods.

[50] In the future, a key task is to find methods that give physically correct entrainment rates, as discussed earlier, and are computationally efficient. This may involve exploring other advection methods, both tracer-based and grid-based. Several grid-based methods exist for treating sharp interfaces or shocks [e.g., *Harten et al.*, 1987; *Muller*, 1992].

[51] Tracer-based advection could be applied to other fields, such as temperature. In that case, each tracer carries the actual value of the field at its location. This approach is particularly suitable for smoothly varying fields such as temperature, and is commonly used for such in the broader modeling community [e.g., *Brackbill*, 1991; *Monaghan*, 1985; *Munz et al.*, 1999; *Sulsky et al.*, 1995]. Diffusion and other processes that involve interaction between tracers are calculated in grid space each time step and interpolated to tracer positions. The ratio method tested here can be viewed as a special case of this method with tracers carrying 0 or 1, and zero diffusion.

Acknowledgments

[52] The authors thank W-S Yang and J.R. Baumgardner for introducing them to the ratio method, Peter van Keken for advocating proper testing of the method and suggestions during review, and an anonymous AE for useful comments. Supported by the David and Lucile Packard Foundation.

References

Brackbill, J. U., FLIP MHD: A particle-in-cell method for magnetohydrodynamics, *J. Comput. Phys.*, *96*, 163–192, 1991.

Christensen, U. R., and A. W. Hofmann, Segregation of subducted oceanic crust In the convecting mantle, *J. Geophys. Res.*, *99*, 19,867–19,884, 1994.

Davaille, A., Simultaneous generation of hotspots and superswells by convection in a heterogeneous planetary mantle, *Nature*, *402*, 756–760, 1999a.

Davaille, A., Two-layer thermal convection in miscible viscous fluids, *J. Fluid Mech.*, *379*, 223–253, 1999b.

Hansen, U., and D. A. Yuen, Extended-Boussinesq thermal-chemical convection with moving heat sources and variable viscosity, *Earth Planet. Sci. Lett.*, *176*, 401–411, 2000.

Harlow, F. H., and J. E. Welch, Numerical calculation of time-dependent viscous incompressible flow of fluid with free surface, *Phys. Fluids A*, *8*, 2182–2189, 1965.

Harten, A., B. Engquist, S. Osher, and S. R. Chakravarthy, Uniformly high order accurate essentially non-oscillatory schemes, III, *J. Comput. Phys.*, *71*, 231–303, 1987.

Hughes, T. J. R., *The Finite Element Method: Linear Static and Dynamic Finite Element Analysis*, 682 pp., Dover, Mineola, N.Y., 2000.

Kellogg, L. H., B. H. Hager, and R. D. van der Hilst, Compositional stratification in the deep mantle, *Science*, *283*, 1881–1884, 1999.

King, S. D., A. Raefsky, and B. H. Hager, Conman - vectorizing a finite-element code for incompressible 2-dimensional convection in the Earths mantle, *Phys. Earth Planet. Int.*, *59*, 195–207, 1990.

Lenardic, A., and W. M. Kaula, A numerical treatment of geodynamic viscous-flow problems involving the advection of material interfaces, *J. Geophys. Res.*, *98*, 8243–8260, 1993.

Monaghan, J. J., Particle methods for hydrodynamics, *Comp. Phys. Rep.*, *3*, 71–124, 1985.

Muller, R., The performance of classical versus modern finite-volume advection schemes for atmospheric modeling in a one-dimensional test-bed, *Mon. Weather Rev.*, *120*, 1407–1415, 1992.

Munz, C. D., R. Schneider, E. Sonnendrucker, E. Stein, U. Voss, and T. Westermann, A finite-volume particle-in-cell method for the numerical treatment of Maxwell-Lorentz equations on boundary-fitted meshes, *Int. J. Numer. Methods Eng.*, *44*, 461–487, 1999.

Ogawa, M., Coupled magmatism-mantle convection system with variable viscosity, *Tectonophysics*, *322*, 1–18, 2000.

Smolarkiewicz, P. K., A fully multidimensional positive definite advection transport algorithm with small implicit diffusion, *J. Comp. Phys.*, *54*, 325–362, 1984.

Sulsky, D., Z. Shi-Jian, and H. L. Schreyer, Application of a particle-in-cell method to solid mechanics, *Comp. Phys. Comm.*, *87*, 236–252, 1995.

Tackley P. J., Effects of strongly variable viscosity on three-dimensional compressible convection in planetary mantles, *J. Geophys. Res.*, *101*, 3311–3332, 1996.

Tackley, P. J., Three-dimensional simulations of mantle convection with a thermochemical CMB boundary layer: D″?, in *The Core-Mantle Boundary Region*, *Geodyn. Ser.*, vol. 28, edited by M. Gurnis et al., pp. 231–253, AGU, Washington, D. C., 1998.

Tackley, P. J., Strong heterogeneity caused by deep mantle layering, *Geochem. Geophys. Geosyst.*, *3*(4), 1024, doi:10.1029/2001GC000167, 2002.

Tackley, P. J., D. J. Stevenson, G. A. Glatzmaier, and G. Schubert, Effects of multiple phase transitions in a three-dimensional spherical model of convection in Earth's mantle, *J. Geophys. Res.*, *99*, 15,877–15,901, 1994.

Ten, A., D. A. Yuen, Y. Y. Podladchikov, T. B. Larsen, E. Pachepsky, and A. V. Malevsky, Fractal features in mixing of non-Newtonian and Newtonian mantle convection, *Earth Planet. Sci. Lett.*, *146*, 401–414, 1997.

van Keken, P. E., S. D. King, H. Schmeling, U. R. Christensen, D. Neumeister, and M. P. Doin, A comparison of methods for the modeling of thermochemical convection, *J. Geophys. Res.*, *102*, 22,477–22,495, 1997.

Zienkiewicz, O. C., and R. L. Taylor, *The Finite Element Method*, 1440 pp., John Wiley, New York, 2000.